Proc. Indian natn. Sci. Acad., **60**, A, No. 1, 1994, pp. 139-155.

A NUMERICAL SIMULATION STUDY OF THE ROLE OF SEA SURFACE TEMPERATURE IN TROPICAL CYCLONE EVOLUTION

D V BHASKAR RAO AND S S V S RAMAKRISHNA

Department of Meteorology & Oceanography, Andhra University, Visakhapatnam-530 003, India

(*Received* 15 *June* 1993; *Accepted* 5 *July* 1993)

The evolution of tropical cyclone circulation from an initial balanced vortex is studied in relation to the sea surface temperature (SST). A six-level axi-symmetric primitive equation model in cylindrical coordinates incorporating the Arakawa-Schubert cumulus parameterization scheme has been used. The SST values have been varied from 298 K to 301 K at one degree interval and the corresponding results indicate that tropical cyclone intensity increases with increase of SST and a minimum SST of 299 K is necessary for the model vortex to transform into a mature cyclone.

Key Words: Numerical Simulation; Sea Surface Temperature; Tropical Cyclone; Evolution; Arakawa-Schubert Cumulus Parameterization Scheme; CISK Mechanism

Introduction

Numerical modelling of tropical cyclones started with the early attempts of Kasahara[1] and Syono[2]. Many modelling studies followed with the development of the concept of CISK mechanism[3], defining the cooperative interaction of cumulus scale and large-scale circulations, which has been the basis of the parameterization of cumulus convection[4-6]. Axi-symmetric models have been designed to derive salient features of the tropical cyclone evolution and are largely successful[7-12]. Anthes[13] gave a good review of the tropical cyclones. Many of the numerical modelling experiments are confined to the simulation of the evolution of cyclones. The pioneering work of Palmen[14] has indicated that the tropical cyclones form over warm tropical oceans where the SST are greater than 26°C and are supported by Wendland[15]. Some attempts have been made to study the development of tropical cyclones in relation to sea surface temperatures using numerical models[16-20]. These model sensitivity studies supported that warm SST favour the intensification of cyclones with a threshold value of 26°C.

The cumulus parameterization scheme proposed by Arakawa and Schubert[6] (A-S scheme) is based on well-formulated physical processes of cloud formation and with a closure hypothesis dependent on the concept of quasi-equilibrium assumption between the cloud generating kinetic energy from large scale forces and the environmental stabilization due to clouds. Wada[11] first attempted the simulation of tropical cyclone using a simplified A-S scheme in which the mixed layer moist static energy (Hm) varies with an assumed constant heat supply. Bhaskar Rao[12] modified Wada's model by incorporating the computation of Hm. In this study, an attempt has been made to study the evo-

lution of the cyclonic circulation in relation to SST values 298, 299, 300 and 301 K using an axi-symmetric primitive equation model in order to study the changes in the evolution at different SSTs and to assess the model's performance in validating the threshold value of SST at 299 K.

Description of the Model

The model used in this study is an axi-symmetric primitive equation model written in r, θ, z, coordinates. The main equations of the model are as follows:

Equation for the radial wind V_r

$$\frac{\partial V_r}{\partial t} = -V_r\frac{\partial V_r}{\partial r} - W\frac{\partial V_r}{\partial z} + \left[f + \frac{V_\theta}{r}\right]V_\theta - \theta\frac{\partial \Phi}{\partial r} + \kappa\left[\nabla_1^2 - \frac{1}{r^2}\right]V_r + \frac{1}{\bar{\rho}}\frac{\partial \tau_r}{\partial z} \quad \ldots (1)$$

Equation for the tangential wind V_θ

$$\frac{\partial V_\theta}{\partial t} = -V_r\frac{\partial V_\theta}{\partial r} - W\frac{\partial V_\theta}{\partial z} + \left[f + \frac{V_\theta}{r}\right]V_r - \theta\frac{\partial \Phi}{\partial r} + \kappa\left[\nabla_1^2 - \frac{1}{r^2}\right]V_r + \frac{1}{\bar{\rho}}\frac{\partial \tau_\theta}{\partial z} \quad \ldots (2)$$

Equation for Potential Temperature (Thermodynamic equation)

$$\frac{\partial \theta}{\partial t} = -V_r\frac{\partial \theta}{\partial r} - W\frac{\partial \theta}{\partial z} + \frac{1}{\bar{\rho}\bar{\Phi}}\left[M_c\frac{\partial s}{\partial z} + D(s_c - s - L\hat{l}_c)\right] + \frac{L}{\bar{\Phi}}C + \kappa_\theta\nabla_1^2\theta \quad \ldots (3)$$

Equation for mixing ratio of water vapour

$$\frac{\partial q}{\partial t} = -V_r\frac{\partial q}{\partial r} - \omega\frac{\partial q}{\partial z} + \frac{1}{\bar{\rho}}\left[M_c\frac{\partial q}{\partial z} + D(q_c - q + \hat{l}_c)\right] - C + \kappa_q\nabla_1^2 q \quad \ldots (4)$$

Equation for continuity of mass

$$\frac{\partial}{\partial z}\bar{\rho}\omega = -\frac{1}{r}\frac{\partial}{\partial r}\bar{\rho}rV_r \quad \ldots (5)$$

Hydrostatic equation

$$\frac{\partial \Phi}{\partial z} = -\frac{g}{\theta}, \quad \ldots (6)$$

where

$$\Phi = C_P\left(\frac{P}{P_0}\right)^{R/C_P}, \quad \ldots (7)$$

$$\nabla_1^2 = \frac{\partial^2}{\partial r^2} + \frac{1}{r}\frac{\partial}{\partial r}.$$

Explanation for the symbols used in given in Table I. Over bars denote functions of height alone and subscript c denotes values in the cloud. Over cap$\hat{}$ denotes values at the clould top level. The cumulus convection effects are included as 3rd and 4th terms in the eq. (3) and (4).

Table I

Description of the symbols

V_r	— radial wind component
V_θ	— tangential wind component
W	— vertical velocity
θ	— potential temperature
q	— mixing ratio of water vapour
l	— mixing ratio of the liquid water
p	— pressure
p_0	— 1000mb
ρ	— density of the air
f	— coriolis parameter
g	— acceleration due to gravity
R	— gas constant for air
L	— latent heat of condensation
C_p	— specific heat of air at constant pressure
S	— dry static energy
$M_B(Z)$	— total vertical cloud mass flux at level Z
D	— total detrainment of cloud mass flux at level Z
C	— large scale condensation per unit time and unit mass.
K	— horizontal eddy viscosity coefficient
K_θ	— horizontal eddy thermal diffusivity
K_q	— horizontal eddy moisture diffusivity

*mps	— meters per second.
*cmps	— centimeters per second.
*hr	— hour/hours.
*km	— kilometers.

$$\tau_r = \bar{\rho}\theta \frac{\partial V_r}{\partial z}, \quad \tau_\theta = \bar{\rho}\theta \frac{\partial V_\theta}{\partial z}. \qquad \ldots (8)$$

At the surface, $\tau_{rs} = \rho_s C_D \mid V_s \mid \theta_{rs}, \quad \tau_{rs} = \rho_s C_D \mid v_s \mid \theta_{rs}$ $\ldots (9)$

C_D is the drag coefficient. Subscript s denotes surface values.

For computational accuracy ϕ and θ are divided into basic and perturbation components. The mixed layer equations are written as follows:

$$\frac{\partial S_M}{\partial t} = - V_r \frac{\partial S_M}{\partial r} + \kappa_H \nabla_1^2 S_M + F_s \qquad \ldots (10a)$$

and

$$\frac{\partial q_M}{\partial t} = -V_r \frac{\partial q_m}{\partial r} + \kappa_H \nabla_1^2 q_M + F_q, \qquad \ldots (10b)$$

where S_M and q_m are the mixed layer values of dry static energy and mixing ratio. F_S and F_q are the sensible and latent heat supplies from the ocean surface given by the bulk aerodynamic formulae

$$F_s = C_D \mid V_s \mid C_P(T_s - T_M)/Z_B \quad \text{and} \quad F_q = LC_D \mid V_s \mid (q_s - q_M)/Z_B, \qquad \ldots (11)$$

where

T_s = temperature at the sea surface
T_M = temperature of air at the sea surface in the mixed layer, and
q_s = mixing ratio at sea surface which is calculated as the saturated mixing ratio at the temperature of the sea surface and existing pressure at that point.

Suffix M denotes values in the mixed layer and z_B is the height of the mixed layer.

Boundary Conditions: To determine pressure field though mass continuity equation, vertical velocity W is taken as zero at $z = 0$ and at $z = z_{top}$ i.e., at the bottom and the top of the model atmosphere.

At the lateral boundaries

$$V_r = V_\theta = 0 \text{ at } r = 0 \text{ and } r = r_{max} \qquad \ldots (12)$$

and

$$\frac{\partial \Phi}{\partial r} = \frac{\partial \theta}{\partial r} = \frac{\partial q}{\partial r} = 0 \quad \text{at } r = 0 \text{ and } r = r_{max} \qquad \ldots (13)$$

r_{max} is the radius of the outer periphery of the computational domain which is taken as 2500km in this model.

Arakawa-Schubert Parameterization Scheme: In this model discretized version of Arakawa and Schubert scheme (AS scheme) is used. The cloud base is fixed at 0.5km and three types of clouds with their tops fixed at 4km, 8km and 12km are only possible because of the vertical resolution as shown in Fig. 1. For each cloud type the cloud base mass flux is defined at half integer levels and entrainment or detrainment takes place at the integer levels. The entrainment rate of each cloud type is calculated with the cloud tops fixed as mentioned earlier. At every time step the convection computations are performed. For the computation of entrainment rate and cloud work function the temperature, the moisture field and the moist static energy are used. A cloud can exist only if the entrainment rate is positive and the virtual static energy in the cloud exceeds the environment value at all levels. When these conditions are satisfied, the equation for the cloud base mass flux is solved. Details of this procedure are same as given in Lord *et al.*[21]

Finite difference Scheme: The vertical structure of the model is given in Fig. 1. The atmosphere is divided into five layers, each layer bound by half-integer. V_r, V_θ and ϕ are defined at integer levels while W, θ and q are defined at half integer levels. The layer between levels 1 and $1\frac{1}{2}$ is the mixed layer. An

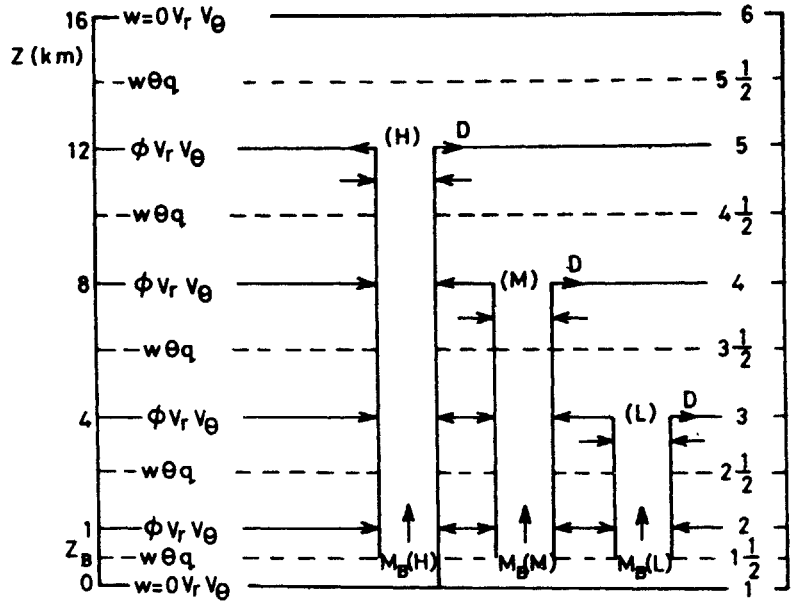

Fig 1 Vertical structure of the model

infinitesimal thin layer is assumed between $Z_{1\frac{1}{2}}$ level and the top of the mixed layer and S_M and q_M are taken as cloud base values. Equations of motion are applied at integer levels and the thermodynamic equation and the water vapour mixing ratio equation are applied at half integer levels. The horizontal computational domain is divided into 21 concentric rings (Table II). The six dependent variables are placed in staggered manner with V_r and V_θ defined at

Table II

Description of the grid points

Grid No.	Distance (km.)	Grid No.	Distance (km.)
1	20	12	443
2	40	13	538
3	60	14	651
4	80	15	787
5	102	16	951
6	128	17	1147
7	160	18	1382
8	198	19	1665
9	244	20	2004
10	298	21	2500
11	364		

integer points while W, θ, q and P are placed at half integer points. Upstream finite differencing is used for space differentiation. Time staggering is used for time derivative with θ, q and ϕ defined at $T\Delta T$ time intervals, while V_r, V_θ and W are defined at intermediate points as $(T+\frac{1}{2})\Delta T$. A time step of 300secs is used to avoid computational instability.

Initial Conditions

For all the experiments in the present study, the initial state is same and designed to have a weak balanced vortex in the wind field. This is obtained through a perturbation in the potential temperature field given by equation

$$\theta'(r_1, Z) = 0.16\left\{\cos\left(\frac{\pi}{r_0}\right)r + 1.0\right\}\sin\left\{\frac{\pi}{Z_T}Z\right\} \quad \ldots (14)$$

for $r < r_0$, where r = radius; r_0 = 200km; Z = height; Z_T = upper boundary of the model atmosphere.

The initial pressure is derived from the hydrostatic equation and the wind from the gradient wind equation. The above perturbation yields a weak balanced circulation with a maximum tangential wind of 8mps at 128km from the centre at the 0km and 1km levels. The tangential wind decreases linearly with height and becomes zero at the 16km level, the model top. The tangential wind at the surface is about 5mps between 60km and 160km and is zero beyond 198km. The radial winds are zero everywhere intially. The initial surface pressure is 1010mb beyond 221km and gradually decreases to 1008.5mb at the 10km radius. The potential temperature perturbation is maximum with an in-

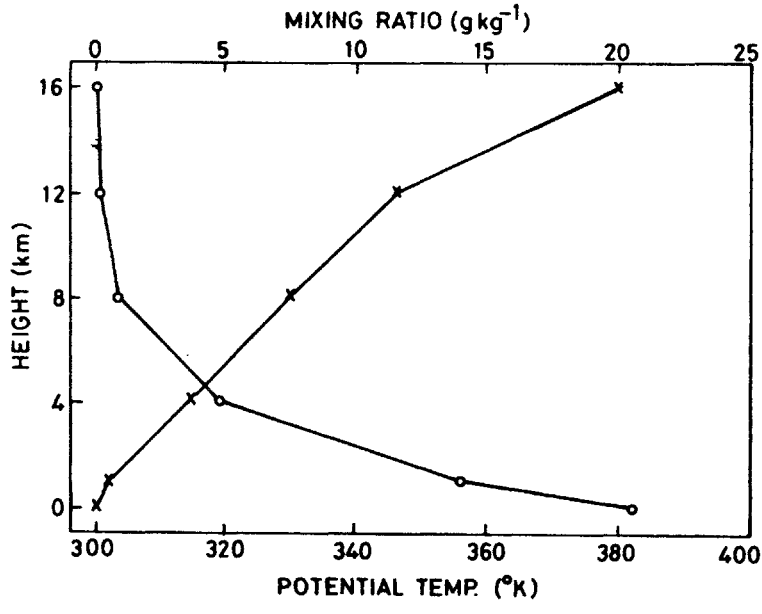

Fig 2 Vertical distributions of potential temperature (cross) and water vapour Mixing ratio (circle)

crease of 0.42K at 10km level. The initial vertical distributions of potential temperature and water vapour mixing ratio are the same as of the mean tropical atmosphere sounding of Jordan[22] and are shown in Fig. 2. The corresponding moist static energy, and saturation moist static energy are given in Fig. 3. This atmospheric state is conditionally unstable with lapse rates exceeding the moist adiabatic lapse rate upto 4km level and then moist adiabatic upto 8km and above 8km stability increases gradually.

The initial mixing ratio values are uniform horizontally. Values of dry static energy (S_m) and the mixing ratio (Q_m) in the mixed layer are computed from the surface values which gives the moist static energy in the mixed layer (H_m), an initial value of 84.5 cal/gm.

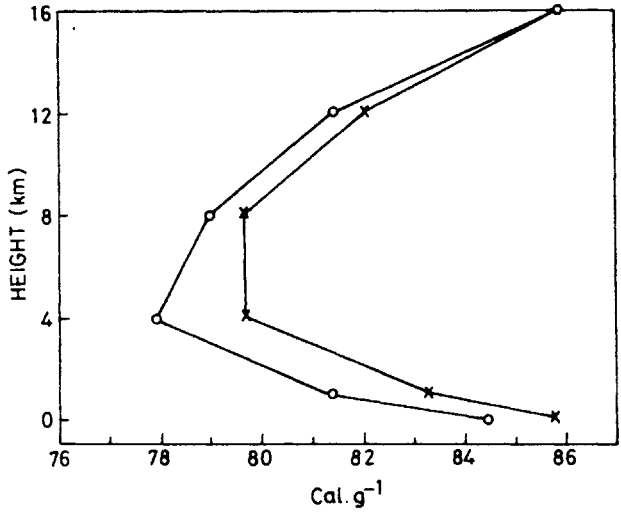

Fig 3 Vertical distributions of moist static energy (circle) and saturation moist static energy (cross)

Results

In this section results obtained from different experiments with SST values of 298K, 299K, 300K and 301K have been presented. The evolution of the circulation from the initial weak vortex in all the four experiments are compared to assess the model sensitivity and also to study the role of SST on the evolution of cyclonic circulation. In the following description experiments are referred to as Experiments I, II, III and IV to correspond with those of SST as 298K, 299K, 300K and 301K respectively.

The variation of the central surface pressure (CSP) with time in all the four experiments are presented in Fig. 4. In Experiment I the CSP reduced gradually till 24hr, then decreased steeply reaching a minimum of 981mb after 42hr period. In Experiment II, steep fall of CSP occurred after 18hr, reaching a minimum of 972mb after 48hrs. In Experiment III, the sharp fall of CSP started after 12hr reaching a minimum of 966mb after 42hr. In Experiment IV, the trend is similar as in the experiment with 300K. The first stage of gradual

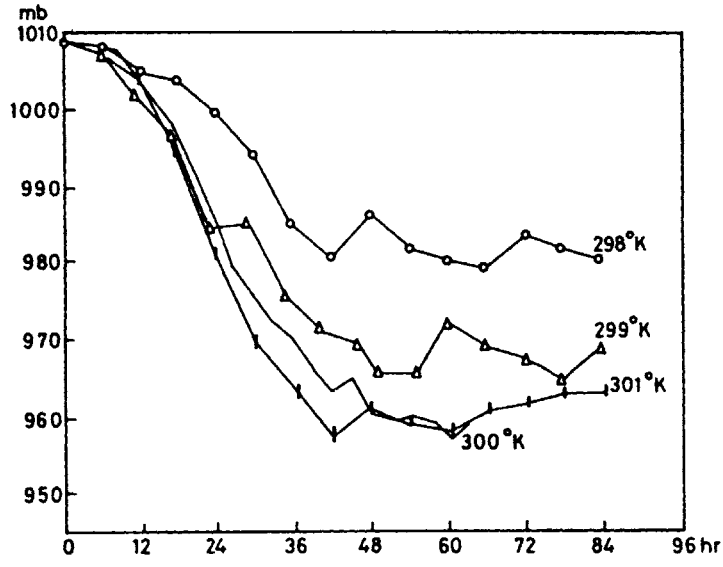

Fig 4 Time variation of central surface pressure (mb) for the four experiments with different SSTs

decrease of GSP corresponds to the pre-developing stage; the steep decrease of the CSP corresponds to the deepening stage and little variation of the CSP after reaching the minimum corresponds to the mature stage.

The time-radius sections of the tangential winds at 1km level for all the four experiments are shown in Fig. 5. In Experiment I (Fig. 5a) the distribution shows that the tangential winds reached a maximum of 33mps at 48hr at 60km radius. The core of the maximum is confined to the central 100km with the maximum occurring during 30hr to 70hr. In Experiment II (Fig. 5b), the tangential winds show a maximum of 39mps at 48hr and the maximum shows outward expansion till mature stage and inward slope later. In Experiment III (Fig. 5c) it is observed that the cyclonic winds reached an intensity of 42mps at 48hr at 100km radius. The tangential winds are noted to be stronger than the two previous experiments. In Experiment IV (Fig. 5d), the tangential winds reached a maximum of 40mps at 36hr. The maximum tangential wind moves inward towards the centre during the deepening stage and outwards later.

The structure of the circulation during the evolution of the vortex is presented corresponding to the mature stage only for all the four experiments. However, the results corresponding to the developing stage, though not presented, are referred to in the description to compare with the results. The height-radius sections of the tangential wind, radial wind, vertical velocity, potential temperature deviation and relative humidity are presented corresponding to the mature stage.

Experiment I (SST= 298K)

The features at the mature stage (*M*-stage) corresponding to this experiment are presented in Fig. 6. The tangential winds (Fig. 6a) show cyclonic circulation throughout the troposphere with a maximum of 30mps at 80km radi-

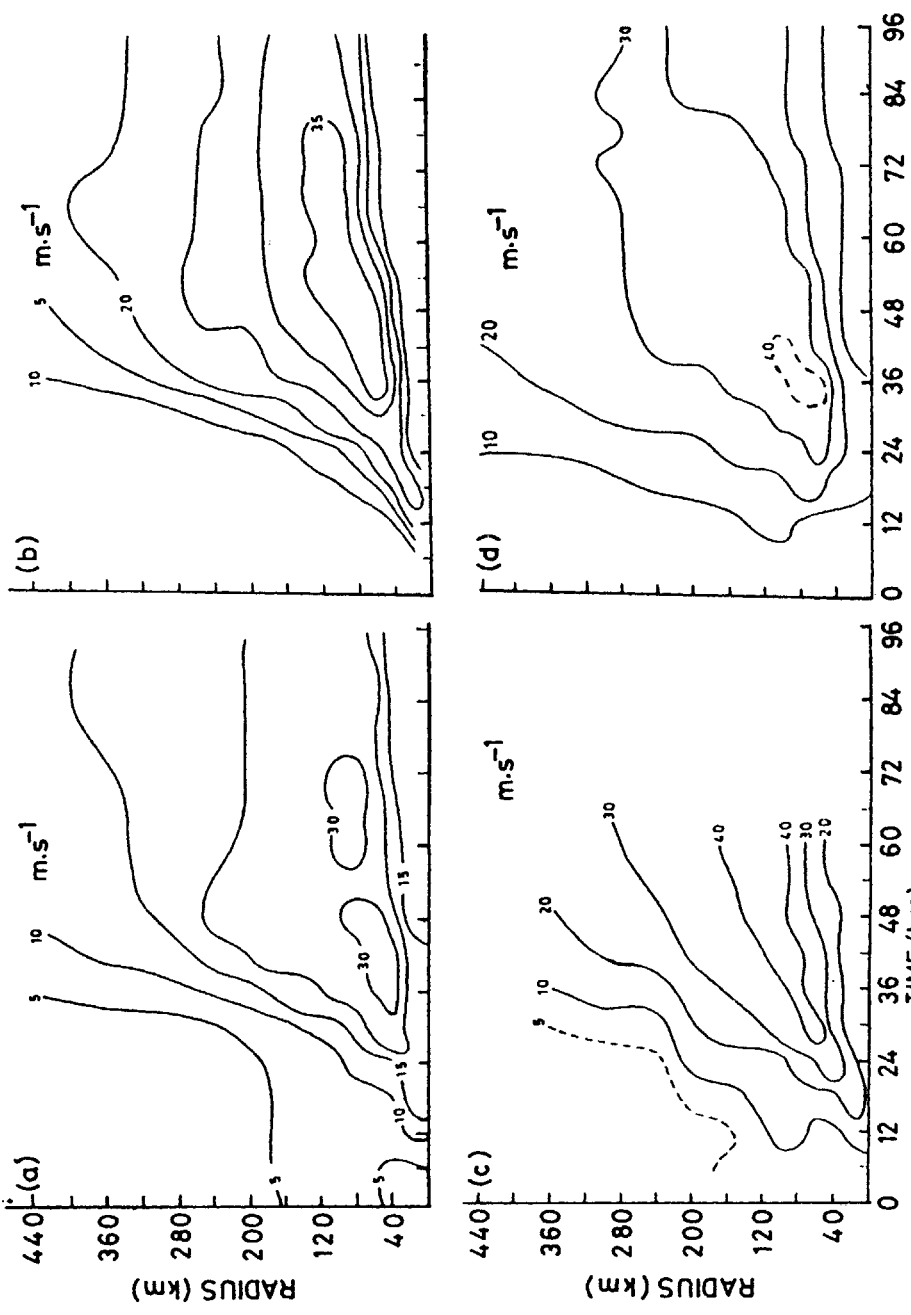

Fig 5 Time-radius section of tangential winds (mps) at 1km level for experiments with SST equal to (*a* 298K; (*b*) 299K; (*c*) 300K and (*d*) 301K

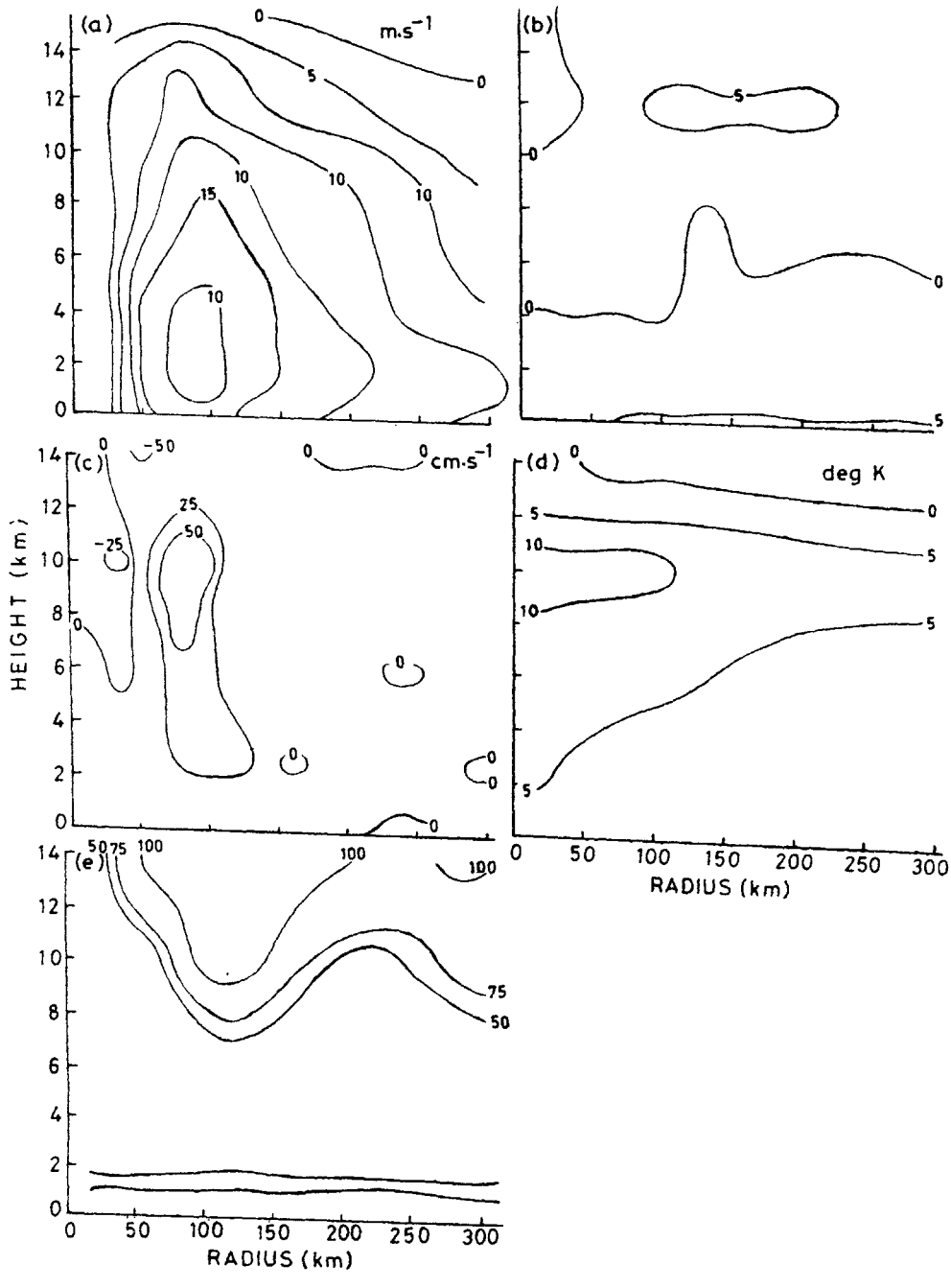

Fig 6 Height-radius distribution at mature stage of (*a*) Tangential wind (mps); (*b*) Radial wind (mps); (*c*) Vertical Velocity (cmps); (*d*) Potential temperature deviation (*K*) and (*e*) Relative humidity (%) for experiment – I i.e., SST = 298K

us in the lower troposphere. A weak anticyclonic circulation is found at very high levels. The radial wind field (Fig. 6b) shows inflow at lower levels and the outflow at higher leves, both with a strength of 5mps, showing a decrease from the developing stage. The vertical motion field (Fig. 6c) shows descending motion at the centre and vertical motion beyond 40km radius. The ascending motion which was very strong during the developing stage with intensities of 200cmps in respect of upward and downward motions decreased in strength of 50cmps after the mature stage. The strong ascending motion over a large region with subsidence at the centre indicates eye formation at the centre. The temperature field (Fig. 6d) shows heating throughout the troposphere with a maximum of 10K in the centre at the 8-10km height. The relative humidity field (Fig. 6e) shows drying at the centre throughout the core of the cyclone which corresponds to the subsidence. At higher levels moist region with 100% relative humidity is observed which coincides with the outflow region. However, there is a dry region in the lower troposphere with relative humidity less than 80%. This region of dryness in the region of convection is not realistic and is to be attributed to the cumulus induced subsidence effect of the Arakawa-Schubert scheme.

Experiment II ($SST = 299K$)

The structure of the circulation at mature stage is presented in Fig. 7. The radius-height section of the tangential winds (Fig. 7a) shows that the cyclonic circulation is found to extend throughout the troposphere with a maximum of 39mps at 80km radius in the lower troposphere. A weak anticyclonic circulation is found at the uppermost level. The radial wind field (Fig. 7b) shows that both the outflow and inflow decreased from the developing stage. The maximum outflow region with 10mps is found at 12km height at a radial distance beyond 240km from the centre. The vertical motion field (Fig. 7c) shows strong descending motion at the centre with a maximum of 180cmps and a vertical motion beyond 40km with a maximum of 100cmps. This indicates the formation of eye. The temperature field (Fig. 7d) shows warming with the maximum reaching 15K at 10km height at a radial distance of 60km. The relative humidity field (Fig. 7e) shows drying in a narrow column throughout the core of the cyclone up to 11km which corresponds to the area of subsidence. At higher levels moist regions with relative humidity values of 100% are observed which can be attributed to the presence of an outflow region. In the lower troposphere, regions with less than 25% humidity are found and this unrealistic feature of dryness at lower levels, is also noted in previous experiment.

Experiment III ($SST = 300K$)

The structure of the vortex at the mature stage i.e., at 48hr is shown in Fig. 8. The radius-height section of the tangential winds (Fig. 8a) shows that the tangential winds increased in strength reaching 43mps at 100km radius. This shows a shift of the maximum from 50km at developing stage to 100km at the mature stage. The cyclonic circulation extended throughout the vertical extent with anticyclonic winds occurring at 16km level. The radial wind field (Fig. 8b) clearly shows inflow at the lower levels and outflow at the upper levels. The strength of the outflow maximum decreased from 25mps at the deve-

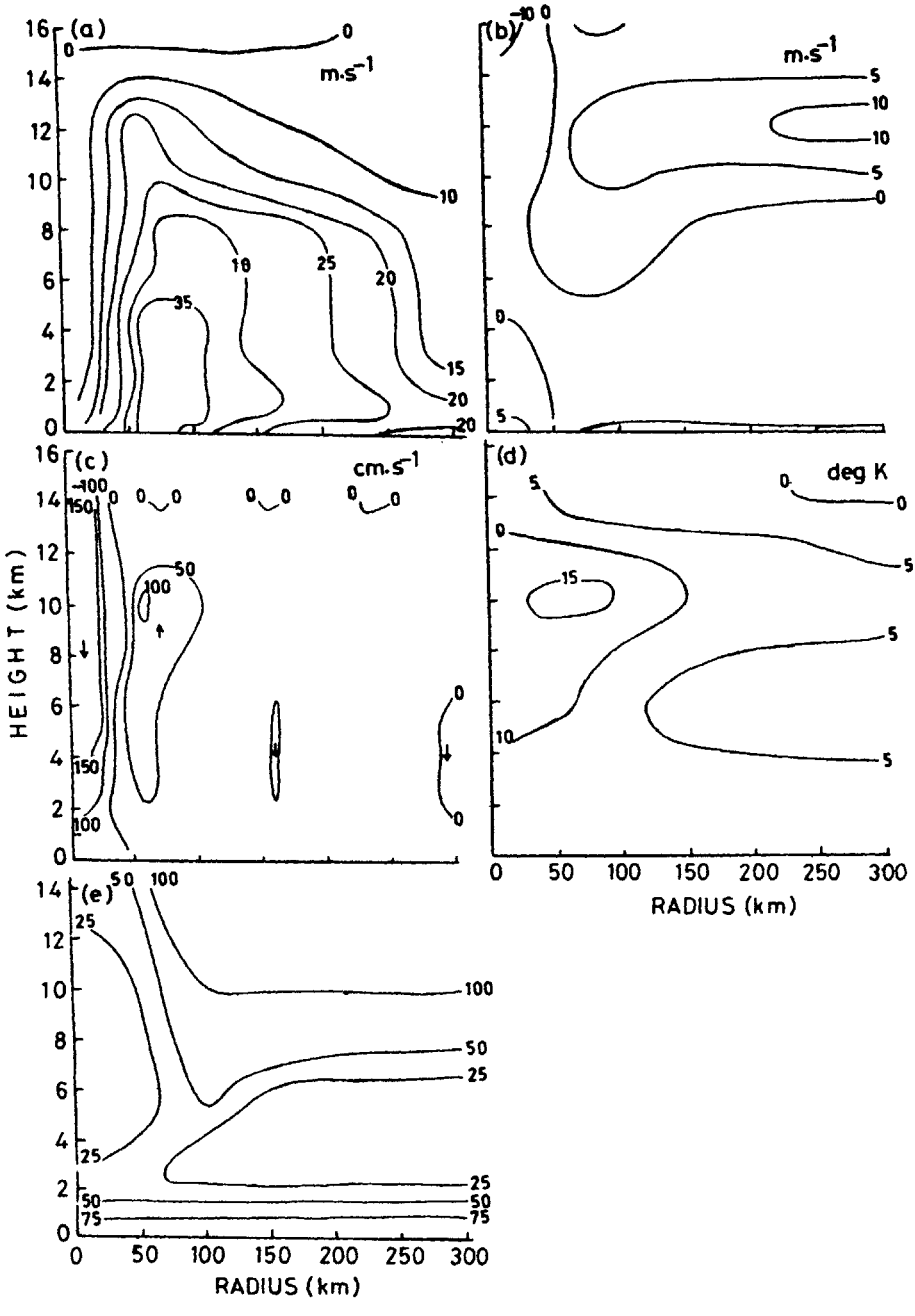

Fig 7 Same as Fig. 6 except for experiment – II i.e., SST = 299K

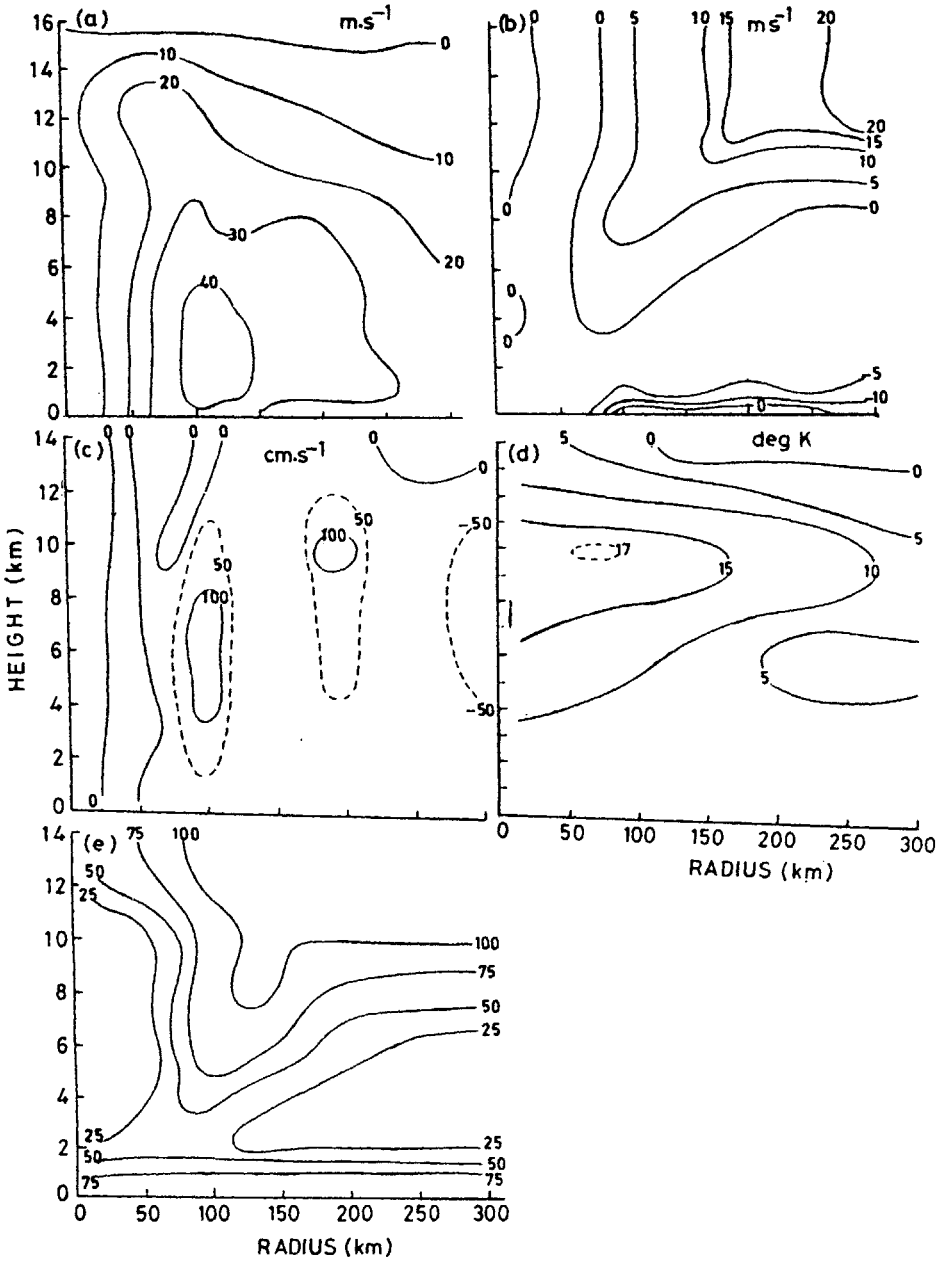

Fig 8 Same as Fig. 6 except for experiment – III i.e., SST = 300K

loping stage to 16mps at the mature stage. The inflow at the lower levels increased considerably from 12mps at the developing stage to 18mps at the mature stage. The vertical motion field (Fig. 8c) shows ascending motion beyond 40km radius and strong descending motion at the centre. This descending motion in conjunction with the absence of convection within the central 60km indicates the eye formation. The potential temperature deviation field (Fig. 8d) shows that maximum warming of 17K takes place at 10km level at a radial distance of 80km. The radial extent of warming also increased at the mature stage. The relative humidity field (Fig. 8e) shows more drying at the centre upto 60km. This is due to the subsidence at higher levels. A moist region which is the result of the outflow is also noted in this experiment and is similar to the one found in the previous experiments. A relatively dry region is found at the lower level of 2.5km is also a feature similar to the previous experiments.

Experiment IV (*SST*= 301 *K*)

The structure of the vortex at 48hr representing the mature stage is given in Fig. 9. It is observed that cyclonic circulation intensified with maximum tang-

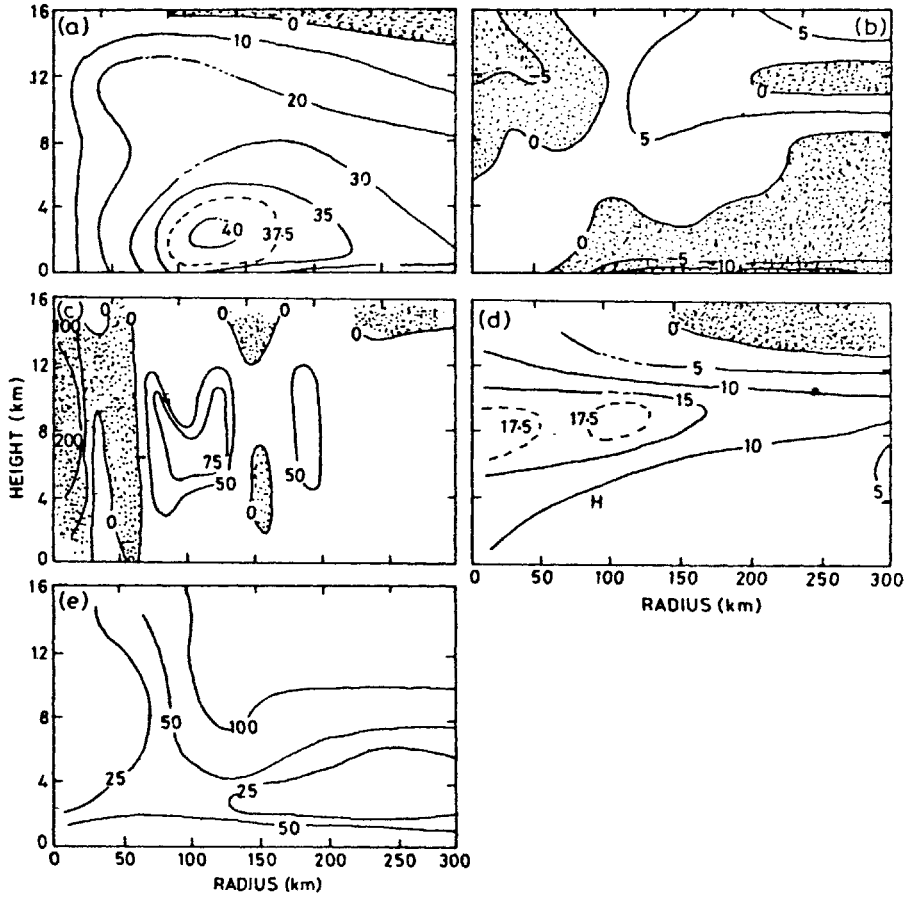

Fig 9 Same as Fig. 6 except for experiment – IV i.e., SST = 301K

ential winds of 40mps (Fig. 9a) observed between 100km and 150km radius indicating a shift from 50km radius at the developing stage. The circulation extended throughout the vertical extent with anticyclonic circulation appearing beyond 100km radius at the uppermost levels. The radial wind field (Fig. 9b) shows clear inflow and outflow regions. The strength of the outflow decreased to a maximum of 5mps from 20mps during the developing stage, while the inflow strength remained same. The vertical motion field (Fig. 9c) shows strong descending motion at the centre with an increase in strength up to a value of 200cmps at the centre. The ascending motion reduced in strength to 75cmps compared to the developing stage but two maxima are still noticed. This also corresponds to the reduction in convection especially in high clouds. The absence of convection at the centre and the strong descending motion clearly demonstrated the formation of the eye at the centre. The temperature field (Fig. 9d) shows further warming of the atmosphere with maximum warming taking place around the 8km level. The two maxima of almost equal magnitude show that the warming due to convection is as effective as the warming due to the strong subsidence at the core. The cold region has moved outward but still could be clearly noticed above the cyclonic circulation. The relative humidity field (Fig. 9e) shows strong drying in a narrow column at the centre within 50km radius corresponding to the region of subsidence. The moist region at higher levels associated with the outflow is also noted, but dry atmospheric condition with relative humidity of 25% is noticed at lower levels. This feature of dryness is similar to the previous experiments.

The time-radius sections of the cloud base flux for H-type clouds for all the four experiments are presented in Fig. 10. In the Experiment I (Fig. 10a) high clouds started from about 18hr corresponding with the developing stage. High clouds with maximum cloud mass flux have been observed from 40-200km after 24hr. In Experiment II (Fig. 10b), it is observed that the high type clouds formed from the beginning with convection values reaching 855gm/m^2/sec. at 24hr at a radius of 60km. The maximum convective region is extended during the mature stage and little convection is observed beyond 160km. In Experiment III (Fig. 10c), it is observed that the high type clouds started from 12hr with maximum cloud base mass flux of 400gm/m^2/sec. at 60km radius at 36hr. In Experiment IV, it is observed (Fig. 10d) that the high type clouds started to form from the initial time with strong convective region at 100km radius. The maximum convection region shifted inward with time concentrating around 50-100km radius during the 24-36hr time period which corresponds to the developing stage.

Summary and Conclusions

The results described above are summarised as follows:

With the increase of SST the intensity of the simulated cyclonic circulation also increased. The minimum CSP attained varied from 981mb to 966mb when the SST increased from 298K to 301K, specifically when the SST increased from 298K to 299K the minimum CSP decreased by about 9mb and for the increase from 299K to 301K the decrease was 6mb. These results

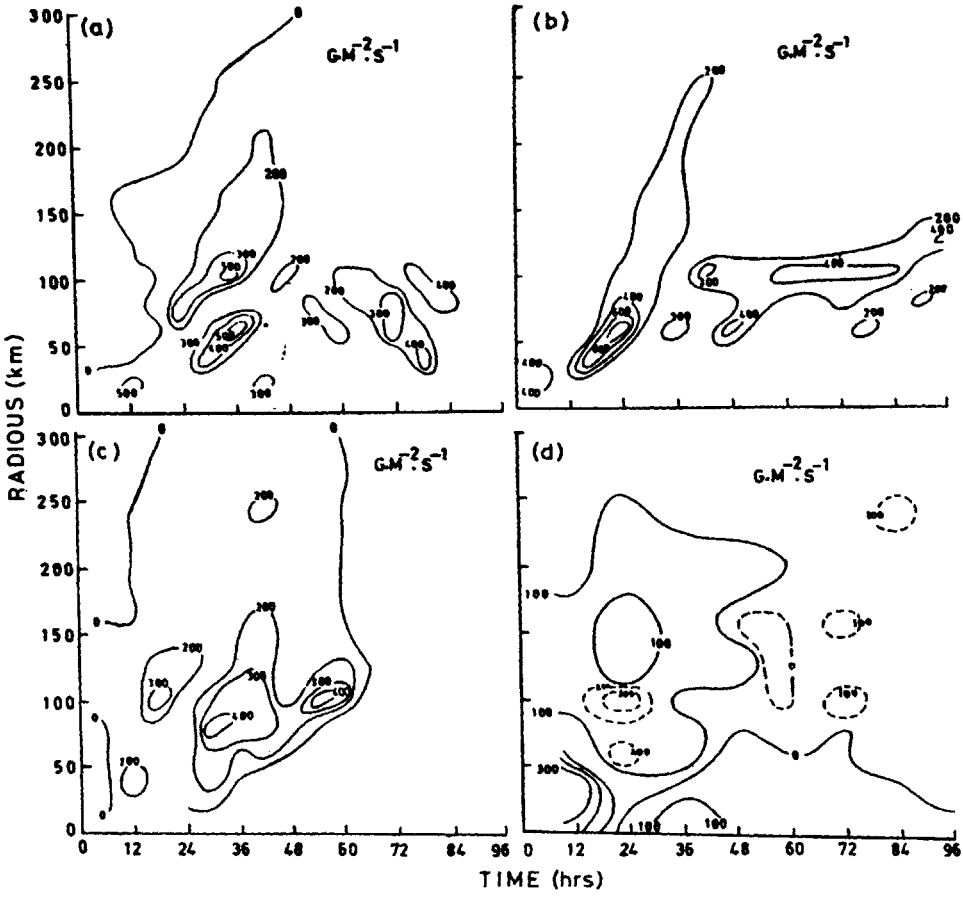

Fig 10 Time-radius section of cloud base mass flux (g m^{-2} s^{-1}) for high clouds for experiments with SSTs equal to (*a*) 298K; (*b*) 299K; (*c*) 300K and (*d*) 301K

agree with those of Sundqvist[17] and Tuleya & Kurihara[20] who found that the largest change in intensity is with SST equal to 300K. Correspondingly the tangential wind at 1km level showed an increase in the attained maximum of 33mps with SST at 298K; 39mps with SST at 299K and 40mps for SST at 300K and 301K. Apart from this the outward extent of the cyclonic circulation has also increased with increase of SST. When the SST has increased from 300K to 301K, the maximum tangential wind has been attained earlier by 18hrs. The evolution of the circulation has shown similar features in all experiments. The important features of the evolution such as the development of the cyclonic circulation, inflow and outflow fields, correspondence with the ascending the descending motions and warm core structure are similar but with variations in strength. However, it is observed that the convective features have been better organized when SST has been increased from 298K to 299K. It is also noticed that the core of the system is warmer with the increase of SST indicating that the convection has increased with the increase of SST.

From the above observed features, it may be inferred that though the broad features of the evolution are similar, it is clear that higher SST values are favourable for the disturbances to grow stronger. It is also noticed that the development of the system has conspicuously changed when the SST has been increased from 298K to 299K indicating that SST values less than 25.8°C are unfavourable for the development of the disturbance into an intense cyclonic system. From the observation that there are little variations in the intensity of the circulation when the SST has increased 300K to 301K it may be inferred that SST values higher than 300K may not be effective in producing stronger cyclonic systems but only be effective for a faster development.

The above experiments indicate that the model used is capable of producing the features of the evolution of cyclonic circulation from a weak vortex. The model is capable to produce changes in the cyclone intensity in relation to SST variation. An important result is that the model derived circulation shows that a conspicuous change when SST increased from 298K to 299K thus upholding that a minimum SST of 26°C is necessary for cyclogenesis. It may also be necessary to use a model with better resolution and to experiment with smaller SST intervals for a better understanding of the associated changes in the cyclone evolution.

Acknowledgement

The authors thank Mr K Ashok for his useful discussions and for his kind help in the preparation of the diagrams and the manuscript. This work has been carried out with the support of DST for a scientific project under grant No. 12(14)84/STP/II dt 8-11-1985.

References

1 A Kashara *J Meteor* **18** (1961) 259-282
2 S Syono *Proc int Symp Num Wea Pred Tokyo* (1962) 405-418
3 J G Charney and A Eliassen *J atmos Sci* **21** (1964) 68-75
4 H L Kuo *J atmos Sci* **22** (1965) 40-63
5 H L Kuo *J atmos Sci* **31** (1974) 1232-1240
6 A Arakawa and W H Schubert *J atmos Sci* **31** (1974) 674-701
7 M Yamasaki *Geophys* **19** (1968) 559-585
8 S L Rosenthal *ESSA Tech Mem ERLTM-NHRL* **82** US Dept. of Commerce. National Hurricane Research Laboratory Miami Fla, USA (1969) 36pp
9 H Sundqvist *Tellus* **22** (1970) 359-390
10 R A Anthes *Mon Wea Rev* **99** (1971) 617-635
11 M Wada *Met Met Soc Japan* **57** (1979) 505-530
12 D V Bhaskar Rao 11 *Nuov Clim* **10C** (1987) 677-696
13 R A Anthes *Meteorol Monogr* **19**(41) (1982) American Meteorological Society 209 pp
14 E Palmen *Geophysica* **3** (1948) 26-38
15 W M Wendland *J appl Met* **16** (1977) 477-481
16 K Ooyama *J atmos Sci* **26** (1969) 3-40
17 H Sundqvist *Tellus* **22** (1970) 504-510
18 S W Chang *Mon Wea Rev* **110** (1979) 2063-2069
19 S W Chang and R V Madala *J atmos Sci* **37** (1980) 2617-2630
20 R E Tuleya and Y Kurihara *Mon Wea Rev* **110** (1982) 2063-2069
21 S J Lord, W C Chao and A Arakawa *J atmos Sci* **39** (1982) 104-113
22 C L Jordan *J Meteor* **15** (1958) 91-97